Approximating electron states in a cylindrical quantum wire with an intrinsic inverse parabolic potential

Gasenna G[1], Maphage L[1], Tshipa M[1]

[1]Theoretical Group, Department of Physics, University of Botswana, Botswana

Abstract

A theoretical investigation on the comparison of electron states obtained from the exact wave functions and those obtained from approximate wave functions is presented. The functions used to approximate the exact wave functions are the parabolic and the cosine functions. For this purpose, oscillator strength for optical transitions in a cylindrical quantum wire due to circularly polarized electromagnetic radiation was evaluated using the exact wave functions and compared with those obtained using the approximate wave functions. These calculations were carried out within the effective mass approximation. The approximate wave functions preserve the functional form of the oscillator strength and other quantum mechanical quantities upon which it depends, namely the electron eigen energies and the interaction integral. Although the approximate wave functions preserve the functional form of the quantum quantities successfully, they fall short in producing accurate magnitudes of the quantum mechanical properties, which is apparent for excited states.

Keywords: Electron States, Cylindrical Quantum Wire, Inverse Parabolic Potential, Approximating Wave Functions.

Introduction

Nanofabrication, the process of making functional structures with patterns in the nanometer region, has been very instrumental in enabling the scientific community to realize nanostructures of all sizes and shapes: quantum dots, quantum wires, thin films and so forth. Top-down and Bottom-up methods are used to build nanostructures. In the Top-down method, nanomaterials are derived from a bulk substrate and obtained by progressive removal of material until the desired nanomaterial is obtained. It is used in the semiconductor industry to fabricate various elements of computer chips. These methods are collectively called lithography (Wang, Fedin, Zhang, & Talapin, 2017) and use a light or electron beam to selectively remove micro-scale structures. In the Bottom-up method, nanostructures are fabricated through a controlled fabrication route that starts from a single atom or molecule. Chemical Vapour Deposition (Zhao, Wei, Gai, Yu, & Ren, 2020) is a Bottom-up method where material to be deposited is firstly heated to its gas form then allowed to deposit as a solid on a surface. Molecular Beam Epitaxy (Zon et al., 2019) is a sophisticated method in which molecular beams interact on a heated crystalline substrate under ultrahigh vacuum to produce single crystal films. Nanostructures have immense applications in a wide range of disciplines. For example, in medicine and biology, they can stimulate, respond to and interact with target cells and tissues in controlled ways, due to their special properties (Xie et al., 2017). Nanostructures also curb the challenge of providing powerful electrochemical energy conversion and storage devices (Zhang, Cheng, & Zhang, 2016).

It is desirable to develop theoretical models for various physical phenomena, including quantum processes in nanostructures. These models assist in comprehending physical processes and in predicting other properties. This is advantageous since different properties can be studied under different conditions (by choosing any desired values of different parameters upon which the studied phenomena depend) without having to fabricate the different nanostructures and performing experiments. The complexity of real systems makes it impossible in some cases to solve physical problems analytically. In such cases, methods of approximation are used. These include neglecting small contributions, and/or replacing the offending term with an approximation that has an analytical solution. The other method would be to approximate the wave function; very good examples were provided by Varshni (1998, 1999). In this way, one utilizes the approximate wave functions to approximate quantum quantities/properties. This has been used particularly in perturbation theory (Brody D. C., Hughston L. P., & J., 2003; Kim, Roznova, Satanin, & Stenberg, 2002; Schilling, Benavides-Riveros, & Vrana, 2017; Sil, Daripa, Kapoor, & Dey, 2017) and variational method

(Sarkar, Sarkar, & Bose, 2018; Yilmaz & Kirak, 2018) (wherein the approximate wave function can be fine-tuned to yield the best possible approximation given the wave function).

This paper has the following organizational structure. Section 2 deals with the theoretical component. The results and discussions can be found in Section 3 while the conclusions are presented in Section 4.

Theory

The envisaged system is a cylindrical nanowire of radius R with an intrinsic inverse parabolic electric confining potential superimposed on an infinite cylindrical quantum well (ICQW), modeled mathematically as

$$V(\rho)=\frac{1}{2}\mu\omega_0^2R^2\left(\frac{R^2}{\rho^2}-1\right), \qquad (\rho<R) \qquad (1)$$

and infinity elsewhere. Here, ω_0 is the angular frequency associated with the classical harmonic oscillator and μ is the effective mass of an electron. This potential profile is very attractive due to its capacity to model cylindrical shells, single- and multi-walled carbon nanotubes. In addition, it can also model a nanostructure with acceptor impurity dopants appropriately nanopatterned by varying the lattice composition of the nanostructure. Due to the symmetry of the problem, cylindrical coordinates are used. Since the Hamiltonian is separable, the wave function can be written in the form

$$\Psi(\rho,z,\phi)=C_{ml}\chi(\rho)Z(z)\Phi(\phi) \qquad (2)$$

where $\chi(\rho)$, $Z(z)$ and $\Phi(\phi)$ are wave functions in the radial, axial and azimuthal directions, respectively and C_{ml} is the normalization constant. The wave function $\Psi(\rho,z,\phi)$ is a solution to the Schrödinger equation. The Schrödinger equation is a quantum mechanical energy conservation law $\hat{p}^2\Psi/(2\mu)+V\Psi=E_{Tot}\Psi$, where E_{Tot} is the total energy of the electron, $\hat{p}=-i\hbar\nabla\ (i^2=-1)$ is the quantum mechanical momentum operator and V is the potential energy of the system. This yields the equation

$$-\frac{\hbar^2\nabla^2}{2\mu}\Psi+V\Psi=E_{Tot}\Psi \qquad (3)$$

in which the Laplacian in cylindrical coordinates has the form

$$\nabla^2=\frac{1}{\rho}\frac{\partial}{\partial\rho}\left(\rho\frac{\partial}{\partial\rho}\right)+\frac{1}{\rho^2}\frac{\partial^2}{\partial\phi^2}+\frac{\partial^2}{\partial z^2} \qquad (4)$$

Using Eqs. (4) and (2) in Eq. (3) and separating variables shows that the azimuthal and axial components of the wave function satisfy the second order differential equations

$$\frac{\partial^2}{\partial\phi^2}\Phi+\frac{2\mu E_\phi}{\hbar^2}\Phi=0 \qquad (5)$$

,

$$\frac{\partial^2}{\partial z^2}Z+\frac{2\mu E_z}{\hbar^2}Z=0 \qquad (6)$$

with E_ϕ and E_z being the azimuthal and axial contributions to the total energy of the system. Solutions to Eqs. (5) and (6) are

$$\Phi(\phi)=C_{1\phi}e^{im\phi}+C_{2\phi}e^{-im\phi}=C_\phi e^{im\phi} \qquad (7)$$

where $m=0,\pm1,\pm2,\ldots$ is the azimuthal quantum number that quantifies quantized angular momentum and

$$Z(z) = C_{1z}e^{ik_z z} + C_{2z}e^{-ik_z z} = C_z e^{ik_z z} \tag{8}$$

with $C_{1\phi}$, $C_{2\phi}$, C_{ϕ}, C_{1z}, C_{2z}, and C_z being constants and k_z the axial wave number of the electron. Quantum states with positive m values are for electrons that have, say, anticlockwise angular momentum while those with negative m values would then be associated with electrons with clockwise angular momentum. Similarly, quantum states with positive k_z values may correspond to electrons moving up the cylindrical quantum wire while those with negative k_z values would therefore be for electrons moving down the cylindrical quantum wire. The radial wave function $\chi(\rho)$ satisfies the second order differential equation

$$\frac{1}{\rho}\frac{d}{d\rho}\left(\rho\frac{d}{d\rho}\chi(\rho)\right)+\left\{\frac{2\mu}{\hbar^2}\left[E_{ml}-\frac{1}{2}\mu\omega_0^2R^2\left(\frac{R^2}{\rho^2}-1\right)\right]-\frac{m^2}{\rho^2}\right\}\chi(\rho)=0 \tag{9}$$

with E_{ml} being the radial confinement energy and l the radial quantum number that specifies the number of nodes a radial wave function has. The solution to the above equation is in terms of the Bessel J functions (Tshipa, 2014),

$$\chi(\rho) = J_{\nu l}(\kappa\rho), \tag{10}$$

where

$$\kappa = \sqrt{2\mu\left(E_{ml}+\frac{1}{2}\mu\omega_0^2R^2\right)\Big/\hbar^2} \tag{11}$$

and

$$\nu = \sqrt{m^2+\mu^2\omega_0^2R^4/\hbar^2}\ . \tag{12}$$

The Bessel Y function has been discarded due to the fact that it diverges at the origin (along the axis of the wire). The potential outside the nanowire is considered to be infinite, hence the electron wave function must vanish at the walls of the nanostructure. Imposing this condition yields the radial energy spectrum for an electron in a cylindrical nanowire with an inverse parabolic potential as

$$E_{ml} = \frac{\hbar^2 j_{0ml}^2}{2\mu R^2}-\frac{1}{2}\mu\omega_0^2R^2 \tag{13}$$

where j_{0ml} are the roots of the Bessel J functions of fractional order. In these investigations, the radial wave function is approximated by the functions

$$\chi_a(\rho) = (\rho/R)^{\sqrt{m^2+\mu^2\omega_0^2R^4/\hbar^2}}\cos\left(\frac{n\pi\rho}{2R}\right) \tag{14}$$

and

$$\chi_b(\rho) = (\rho/R)^{\sqrt{m^2+\mu^2\omega_0^2R^4/\hbar^2}}\left(1-\rho^2/R^2\right). \tag{15}$$

The radial confinement energy associated with the approximate wave functions has been calculated using the expression

$$\left\langle ml\left|-\frac{\hbar^2}{2\mu}\frac{1}{\rho}\frac{d}{d\rho}\left(\rho\frac{d}{d\rho}\right)+\frac{1}{2}\mu\omega_0^2R^2\left(\frac{R^2}{\rho^2}-1\right)+\frac{m^2\hbar^2}{2\mu\rho^2}\right|ml\right\rangle \tag{16}$$

where $\langle ml|\aleph|ml\rangle$ is the usual quantum mechanical expectation value for the quantity $\aleph$. The oscillator strength, which is an index of the strength of a transition, is given by (Tshipa, 2014)

$$f_{m'l'ml} = \frac{2\mu\Delta E R^2}{\hbar^2} I^2_{m'l'ml} \tag{17}$$

where $I_{m'l'ml} = \langle m'l'|\rho|ml\rangle / R$ is the scaled interaction integral coupling the initial state $|ml\rangle$ to the final state $|m'l'\rangle$ and transition energies $\Delta E = E_{m'l'} - E_{ml}$ are the differences in energies of the states between which transitions may occur.

This communication is aimed at introducing some wave functions that can also be utilized to yield functional forms of quantum mechanical quantities in question. In this way, a number of quantities can be explored without using high level mathematics, which include oscillator strengths, binding energies, transition rates, quantum blockade and so forth.

Results and Discussion

The effective electronic mass used in these computations is relevant to GaAs quantum structures, $\mu = 0.067 m_e$, m_e being the free electron mass. The radius of the test quantum wire has been held constant at $R = 150\text{Å}$.

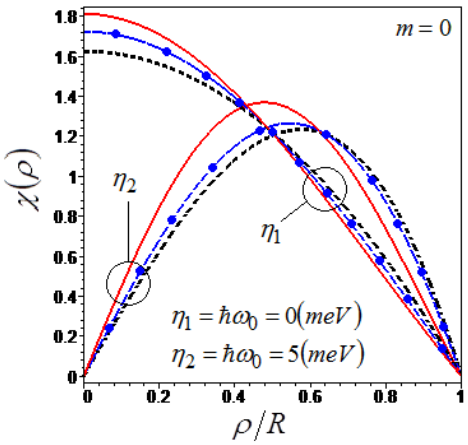

Figure 1. Comparison between the ground state exact wave functions (solid plots) and the approximations given by Eq. (14) (plots with dots) and Eq. (15) (dashed curves), in a cylindrical nanowire of radius $R = 150\text{Å}$. The curves with the highest intercepts are for an infinite cylindrical quantum well (ICQW) while the graphs with least intercepts are for a nanowire with an inverse parabolic potential superimposed on an ICQW

Figure 1 depicts the comparison between approximate electron wave functions and the exact wave functions in a cylindrical quantum wire of radius $R = 150\text{Å}$. The solid plots represent the exact wave functions, the plots with dots were obtained using Eq. (14) χ_a and those obtained by Eq. (15) χ_b have been dashed. The wave functions have been plotted for an ICQW $(\hbar\omega_0 = 0)$, denoted by η_1, and for an inverse parabolic potential superimposed on an ICQW $(\eta_2 = \hbar\omega_0 = 5\ \ meV)$. The inverse parabolic potential expels electrons away from the axis of the nanowire, signified by shifting of peaks of wave functions towards the outer walls of the nanowire. As can be seen in the figure, there is very good agreement between the approximate wave functions and the exact, with the approximate wave function χ_a given by Eq. (14) proving to be a more accurate approximation.

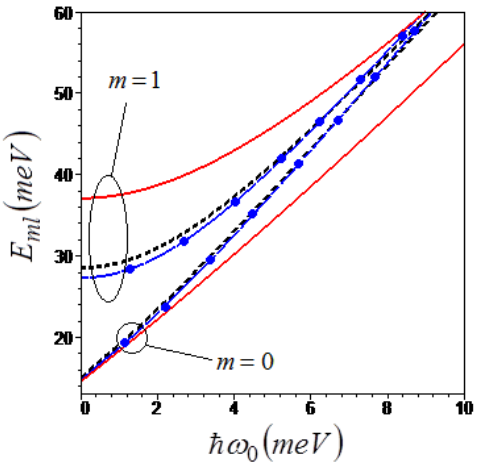

Figure 2. The dependence of the energy eigenvalues on strength of the inverse parabolic potential in a cylindrical quantum wire of radius $R=150\mathring{A}$ for the ground state and the first excited state. Solid plots are the exact values (Eq. 13) while the plots with dots are generated from Eq. (16) using Eq. (14) χ_a as the approximate wave function and the dashed plots are also obtained from using Eq. (16) but using the approximate wave function given in Eq. (15) (χ_b).

The dependence of the energy eigenvalues on the inverse parabolic potential for the ground state and first excited state can be viewed in Fig. 2. The energy eigenvalues obtained from the approximate wave functions portray the same functional form as the exact energy eigenvalues in their variation with the inverse parabolic potential. The approximate wave functions give accurate energy eigenvalues for the ground state, but less accurate values for the excited state. This implies that the approximate wave functions will not be accurate in determining transition energies. The accuracy of the transition energies obtained from the approximate wave functions increases with increasing radius of the nanowire, therefore the approximate wave functions will be more accurate for wide nanowires.

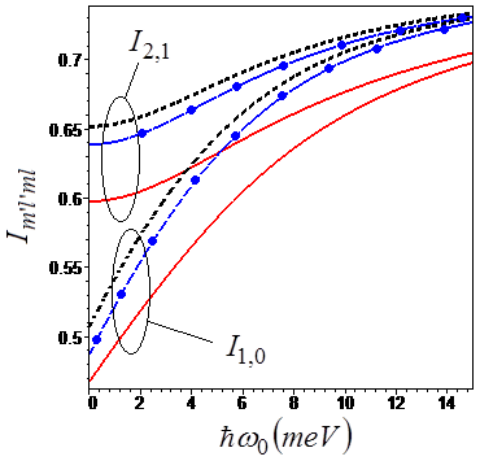

Figure 3. Variation of the scaled interaction integral with the inverse parabolic potential in a cylindrical quantum wire of radius $R=150\mathring{A}$, for transitions from the ground sate $(m=0)$ to the first excited state $(m'=\pm1)$ and from the first excited state $(m=\pm1)$ to the second excited state $(m'=\pm2)$. As regards the different wave functions, the legend in Fig. 2 is adopted.

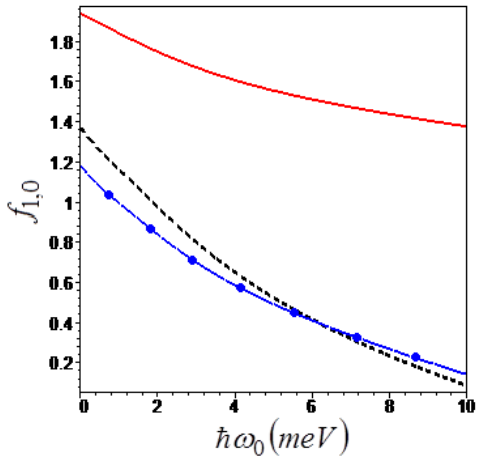

Figure 4. The oscillator strength as a function of strength of the inverse parabolic potential, for transition from the ground state $(m=0)$ to the first excited state $(m'=\pm 1)$. The legend in Fig. 2 is adopted.

Figure 3 illustrates the dependence of the scaled interaction integral on the inverse parabolic potential. The exact results are depicted with solid lines, those of the approximate wave function Eq. (14) χ_a are represented by plots with dots, and those due to Eq. (15) χ_b are depicted by dashed curves. As can be appreciated from the figure, the functional form of the dependence of the interaction integral is preserved by the approximations. However, the accuracy of determining the magnitude of the interaction integral diminishes with increasing m. This preservation of functional forms of these quantum quantities can be found also in the dependence of the oscillator strength on the inverse parabolic potential, shown in Fig. 4. The parameters for this figure are the same as those for Fig. 3. As can be appreciated from the figure, the inverse parabolic potential decreases the magnitude of the oscillator strength, specifically due to the reduction of transition energies as the potential intensifies. As with the interaction integral, the approximations still fall short when it comes to determining the magnitude of the oscillator strength.

Conclusions

Quantum properties of an electron confined in a cylindrical quantum wire with an inverse parabolic potential obtained from approximate wave functions have been compared with those obtained from the exact wave function. The exact wave function was obtained by solving the Schrödinger equation within the effective mass approximation. The approximate wave functions considered here are a parabolic function and a cosine function. Although the approximate wave functions do not yield very accurate magnitudes of quantum properties, they are very successful in preserving the functional forms of the variations of the quantities with the inverse parabolic potential. It should, thus, be possible to use simpler wave functions to obtain a very representative picture of the quantum world. In addition to being used as a tool to approximate the variations of quantum quantities before, say, an experiment or a higher level mathematics calculation is performed, it can be used as a tool to train undergraduate students in the rigors and subtleties of Quantum Mechanics in particular, and theoretical physics as a whole.

Conflicts of Interest

Authors have no conflicts of interest to declare.

Acknowledgements

MT would like to express gratitude to Rorisang W. Tshipa for typing portions of this work.

References

1. Brody D. C., Hughston L. P., & J., S. (2003). Relaxation of quantum states under energy perturbations. Proceeding of the Royal Society A, 459(2037), 2031113.
2. Kim, C. S., Roznova, O. N., Satanin, A. M., & Stenberg, V. (2002). Interference of quantum states in electronic waveguides with impurities. Journal of Experimental and Theoretical Physics, 94, 992-1007.
3. Sarkar, S., Sarkar, S., & Bose, C. (2018). Influence of polarization and self-polarization charges on impurity binding energy in spherical quantum dot with parabolic confinement. Physica B-condensed Matter, 541, 75-78.
4. Schilling, C., Benavides-Riveros, C. L., & Vrana, P. (2017). Reconstructing quantum states from single-party information. Physical Review A, 96. doi: https://doi.org/10.1103/PhysRevA.96.052312
5. Sil, N. K., Daripa, N., Kapoor, A., & Dey, S. K. (2017). Perturbation method for calculating impurity binding energy in an inhomogeneous cylindrical quantum dot with dielectric mismatch. Pramana, 90, 1-6.
6. Tshipa, M. (2014). Oscillator strength for optical transitions in a cylindrical quantum wire with an inverse parabolic confining electric potential. Indian Journal of Physics, 88, 849-853. doi: 10.1007/s12648-014-0501-y
7. Varshni, Y. P. (1998). Simple wavefunction for an impurity in a parabolic quantum dot. Superlatt. Microstruct., 23(1), 145-149.
8. Varshni, Y. P. (1999). Accurate wavefunctions for hydrogenic donors in GaAs(Ga,Al)As quantum dots. Phys. Lett. A, 252, 248-250.
9. Wang, Y., Fedin, I., Zhang, H., & Talapin, D. V. (2017). Direct optical lithography of functional inorganic nanomaterials. Science, 357, 385 - 388. doi: 10.1126/science.aan2958
10. Xie, N., Liu, S., Yang, X., He, X., Huang, J., & Wang, K. (2017). DNA tetrahedron nanostructures for biological applications: biosensors and drug delivery. Analyst, 142(18), 3322-3332. doi: 10.1039/C7AN01154G
11. Yilmaz, S., & Kirak, M. (2018). An investigation on the effect of impurity position on the binding energy of quantum box under electric field with pressure and temperature. International Journal of Modern Physics B, 32, 1850154. doi: 10.1142/S0217979218501540
12. Zhang, X., Cheng, X., & Zhang, Q. (2016). Nanostructured energy materials for electrochemical energy conversion and storage: A review. Journal of Energy Chemistry, 25(6), 967-984.
13. Zhao, X., Wei, C., Gai, Z., Yu, S., & Ren, X. (2020). Chemical vapor deposition and its application in surface modification of nanoparticles. Chemical Papers, 74(3), 767-778. doi: 10.1007/s11696-019-00963-y
14. Zon, Phienlumlert, P., Thainoi, S., Kiravittaya, S., Tandaechanurat, A., Nuntawong, N., . . . Arakawa, Y. (2019). Growth Rate Dependent Properties of GaSb/GaAs Quantum Dots on (001) Ge Substrate by Molecular Beam Epitaxy. Physica Status Solidi (a), 216.